Phase Transition of RNA-protein Complexes into Ordered Hollow Condensates

Ibraheem Alshareedah[§a], Mahdi Muhammad Moosa[§a], Muralikrishna Raju[b], Davit Potoyan*[b], Priya R. Banerjee*[a]

[a]Department of Physics, University at Buffalo, Buffalo NY 14260, USA
[b]Department of Chemistry, Iowa State University, Ames IA 50011, USA

§ These authors contributed equally

*Corresponding Authors: P. R. B.: prbanerj@buffalo.edu; D. P.: potoyan@iastate.edu

Abstract

Charge driven condensation of intrinsically disordered protein-RNA complexes is ubiquitous in both natural and biomimetic systems. So far, isotropic liquid droplets are the most commonly observed topology of RNA-protein condensates in experiments and simulations. Here, by systematically studying the phase behavior of RNA-protein complexes across varied mixture compositions, we report a hollow vesicle-like condensate phase of nucleoprotein assemblies that is distinct from RNA-protein droplets. We show that these vesicular condensates are stable at specific charge disproportionate regimes within the phase diagram and are formed through the self-assembly of highly charged anisotropic protein-RNA complexes. Similar to membranes composed of amphiphilic lipids, these nucleoprotein-RNA vesicular membranes exhibit local ordering, size-dependent permeability, and selective encapsulation capacity without sacrificing their dynamic formation and dissolution in response to physicochemical stimuli. Our findings suggest that protein-RNA complexes can robustly create lipid-free vesicle-like enclosures by phase separation.

Significance statement

Vesicular assemblies play crucial roles in subcellular organization as well as in biotechnological applications. Classically, the ability to form such assemblies were primarily assigned to lipids and lipid-like amphiphilic molecules. Here, we show that complexes of negatively charged RNAs and positively charged disordered polypeptides can form vesicle-like ordered assemblies at charge disproportionate mixture compositions. We also show that the ability to form vesicular assemblies is not specific to RNA-protein complexes, rather is generic to complexes of oppositely charged polyionic chains. We speculate that such vesicular assemblies play crucial roles in the formation of dynamic multi-layered subcellular membrane-less organelles and can be utilized to fabricate novel stimuli-responsive microscale systems.

Keywords: Nucleoprotein assembly, Complex coacervation, Optical tweezer, MD simulation, Biomolecular condensation.

Introduction

Precise spatiotemporal control of biochemical processes is indispensable to life. Classically, it was assumed that amphiphilic lipids provide living systems the capacity to segregate different biological processes into distinct membrane-bound compartments and therefore, afford spatial and temporal separation of (sub)cellular biochemistry (1). These membrane-bound compartments provide an independent internal environment that can be tuned as per cellular needs. Recent advances indicate that, in addition to membrane-bound organelles, cells also utilize membrane-free protein/RNA-rich condensates as compartments for organizing the intracellular space (2-5). These fluid compartments, often referred to as membrane-less organelles (MLOs), are formed by liquid-liquid phase separation (LLPS) and can partition a diverse set of biomolecules selectively (6). One key advantage of these MLOs is their dynamic nature wherein they can rapidly form and dissolve in a stimuli responsive fashion. This directly contrasts highly stable membrane-bound organelles that often persist throughout the lifespan of individual cells.

Since MLOs are phase separated bodies, their internal microenvironment is significantly higher in density as compared to the surrounding cytoplasm/nucleoplasm and exhibit complex fluid-like properties (7). To spatially segregate biochemical processes within this condensed phase, many MLOs [*e.g.*, nuclei (8), nuclear speckles (9), paraspeckles (10), stress granules (11, 12) and P-granules (13)] utilize distinct sub-compartments within themselves. Such multilayered structures are best described by a coexisting multi-phasic condensate model where two or more distinct types of condensates are formed by the LLPS of individual components in a multi-component mixture (5). However, a different class of multilayered MLOs has also been reported, where the layered topology is manifested due to the presence of a hollow internal space. For example, *in vivo* experiments have demonstrated that both nuclear and cytoplasmic germ granules of *Drosophilla* can exhibit hollow morphologies (14-16). In another system, it was observed that simple overexpression of TDP-43, a stress granule protein, can give rise to multilayered compartments with vacuolated nucleoplasm-filled internal space (17). However, physical driving forces behind these hollow morphologies remain poorly understood.

Recently, we demonstrated that RNA can mediate a reentrant phase transition of cationic ribonucleoproteins containing arginine-rich low complexity domains (LCDs) through long-range electrostatic interactions (18, 19). At sub-stoichiometric regime, RNA triggers ribonucleoprotein (RNP) phase separation whereas at super-stoichiometric ratio, excess RNA leads to droplet dissolution due to charge inversion on the surface of RNP-RNA complexes (18). This charge inversion suggests that the stoichiometry of these *fuzzy protein-RNA assemblies* is not fixed but varies with the mixture composition. Interestingly, we observed that sudden jumps in RNA-to-LCD stoichiometry can lead to the formation of transient hollow droplet topologies under non-equilibrium conditions (18). Although, these vacuolated structures were observed only as fleeting intermediates during reentrant dissolution of protein-RNA condensates, their occurrence nevertheless suggested that associative RNA-protein systems may have access to complex morphologies distinct from isotropic liquid droplets. This leads to the following question: are these hollow droplets only kinetic intermediates or are they representative of potentially stable topologies of simple associative two-component condensates?

Here, to ascertain these possibilities, we explore the liquid-liquid phase separation regime within protein-RNA reentrant phase space that spans three orders of magnitude in concentrations. Using a combination of biophysical and computational tools (*e.g.,* confocal microscopy, ensemble spectroscopy, optical tweezers, microfluidic manipulation, and molecular dynamics simulation),

we report a hitherto unknown structural transition from isotropic liquid droplets to a vesicle-like phase in nucleoprotein-RNA condensates. These vesicle-like condensates are hollow structures enclosed by an ordered nucleoprotein-RNA membrane, and are formed via self-assembly of nucleoprotein-RNA complexes under distinct charge disproportionate mixture compositions.

Results and Discussion

Nucleoprotein-RNA complexes form stable hollow condensates with vesicle-like properties

Our previous observations suggested that hollow condensate topology may exist when RNA concentration is substantially higher than RNP concentration (18). To investigate such complex morphologies, we first probed for the mesoscale structure of condensates formed by a model arginine-rich disordered nucleoprotein (20), protamine (PRM, see *SI Appendix*, Fig. S1*A*), with a single-stranded RNA [poly(U)] at excess RNA conditions ($C_{RNA} = 5 \times C_{PRM}$). Remarkably, we observed that stable micron-sized hollow condensates are readily formed at 4.4 mg/ml PRM and 22 mg/ml RNA. These hollow condensates closely resemble lipid vesicles in their appearance (Fig 1*A*). Below 11 mg/ml RNA, PRM-RNA mixture formed spherical liquid droplets that are uniform in density (Fig. 1*A* and *B, SI Appendix*, Fig. S2). Z-stack analysis using confocal fluorescence microscopy revealed that the hollow condensates have a rim and an internal lumen (Fig. 1*C*, *SI Appendix,* Fig. S3). PRM localizes within the rim but not in the lumen. We then asked whether RNA also localizes within the PRM-rich rim or inside the lumen. Two-color confocal microscopy revealed that RNA [probed by SYTO13 which fluoresces when bound to RNA (21)] co-localizes with PRM and is highly enriched in the rim. The lumen appears to be devoid of PRM and RNA as judged by the similar fluorescence intensities to the external dilute phase (Fig 1*D*). To ascertain whether the lumen environment is indeed a *dilute phase* (as classical membrane-enclosed lumen environment is in a lipid vesicle), we measured macromolecule diffusion *outside*, *in the lumens,* and *within the rims* of hollow condensates utilizing fluorescence correlation spectroscopy (FCS). FCS autocorrelation traces clearly show that molecular diffusion is significantly slowed down within the rim (*e.g.,* the diffusion half-time is increased by three orders of magnitude), whereas diffusion remains similar for molecules that are localized in the lumen as those in the external dilute phase (Fig. 1*E*). Collectively, these experimental results indicate that (i) PRM-RNA complexes can form lipid-free vesicular structures at excess RNA-to-PRM ratio ($C_{RNA} > 2.5 \times C_{PRM}$), and (ii) the nucleoprotein membrane-enclosed internal space is a distinct *low-density phase* that is independent of the condensed fluid phase of vesicle rims.

Membranes are usually dynamic. For example, in lipid membranes, molecules diffuse within the membrane rim as a two-dimensional fluid (22). This observation led us to ask whether PRM-RNA vesicle rims also exhibit similar liquid-like properties. Our FCS measurements suggest that the rim is a viscous fluid (Fig. 1*E*). To confirm this liquid-like property of the nucleoprotein membranes, we utilized two orthogonal assays. *First*, we performed a Fluorescence Recovery after Photobleaching (FRAP) experiment wherein we bleached a circular spot within the vesicle rim. FRAP recovery profile showed that the bleached region recovered to ~100% fluorescence intensity within 10 seconds (Fig. 1*F*, Movie S1), suggesting that the hollow condensate's rim is highly dynamic. *Second*, we used optical tweezers to perform controlled fusion of two hollow condensates. Trap-controlled fusion experiments revealed that these hollow condensates fuse to form multi-compartment vesicular structures that rapidly relax into vesicles with single internal

lumen (Fig. 1*G top* panels, Movie S2). This behavior is analogous to fusion of lipid membranes (23, 24). Passive fusion of vesicles was also observed during the initial stages of sample equilibration (*SI Appendix*, Fig. S4). Furthermore, we noticed that the hollow condensates can also fuse with small PRM-RNA spherical droplets suggesting that they contain physicochemically compatible condensed phases (Fig. 1*G bottom* panels, Movie S3). Thus, similar to lipid-bound vesicle rims, nucleoprotein-RNA membranes display a high degree of fluidity. Overall, our results clearly demonstrate that nucleoprotein-RNA complexes can form stable vesicular condensates that are structurally similar to lipid vesicles.

Vesicular structures represent distinct condensed phases of protamine-RNA assemblies

To determine the conditions at which PRM-RNA hollow condensates are stabilized, we mapped the PRM-RNA phase diagram as a function of mixture compositions utilizing optical microscopy and solution turbidity measurements. Briefly, we recorded bright-field and fluorescence micrographs of PRM-RNA samples at a desired composition to determine whether the sample forms droplets, hollow condensates, or a homogeneous mixture. These measurements are summarized as a phase diagram in Figure 2*A*. Our phase diagram shows that PRM-RNA condensation is *reentrant* (see also *SI Appendix,* Fig. S5), which is generally the case for electrostatically driven liquid-liquid condensation (19, 25). *In addition to the RNA excess regime, we observed that hollow condensates appear at PRM excess regime* (open blue circles in Fig. 2*A*). Inspection of the phase diagram superimposed on the net charge concentration (estimated as $Q_{polycation}C_{polycation} - Q_{polyanion}C_{polyanion}$; plotted as a color gradient in Figure 2*A*) reveals that stable hollow condensates are formed when there is substantially excess net charge in the PRM-RNA mixture, regardless of whether this charge is negative (RNA excess) or positive (PRM excess). Electrophoretic mobility measurements indeed confirmed that *at RNA excess conditions, PRM-RNA complexes are negatively charged* and *at protein excess conditions, these complexes are positively charged* (Fig. 2*B* and *SI Appendix*, Fig. S6). Our fluorescence-based molecular partitioning assay suggests that, similar to vesicles under RNA-excess conditions, vesicles under PRM-excess regime also enrich both PRM and RNA within their rims whereas their internal lumen remain mostly devoid of both PRM and RNA (Fig. 2*C*).

Next, we hypothesized that if these nucleoprotein vesicles indeed represent stable states in the phase diagram, then influx or efflux of one of the components should be sufficient to reversibly induce droplet-to-vesicle transformations (Fig. 2*D*). To test this idea, we prepared and flowed PRM-RNA droplets [composed of 0.88 mg/ml PRM and 0.44 mg/ml poly(U)] into a microfluidic flow cell (*SI Appendix*, Fig. S7A). Then, we employed a dual-trap optical tweezer to trap two droplets and transported them to a second channel that was initially filled with buffer and connected to a poly(U) RNA source [poly(U) concentration = 10 mg/ml] (*SI Appendix*, Fig. S7B). This poly(U) concentration is higher than RNA concentration required for a droplet-to-vesicle structural transition under the experimental conditions. Once the flow of RNA started, we observed that the *PRM-RNA droplets spontaneously transitioned to vesicles* (Fig. 2*D*; *SI Appendix*, Fig. S7C; Movie S4), whereas a control experiment with just the experimental buffer (lacking RNA) flow failed to produce a similar effect (*SI Appendix*, Fig. S7C). Contrastingly, when we removed RNA (partial) from preformed PRM-RNA vesicles by RNAse-A treatment, *PRM-RNA vesicles rapidly transitioned to droplets* (Fig. 2*D*; Movie S5). These results clearly indicate that nucleoprotein assemblies can dynamically undergo structural transition between vesicles and droplets via influx and removal of RNAs.

Both arginine and lysine-rich polypeptides form hollow condensates with RNA

The positive charge of protamine is primarily due to the 21 arginine residues (accounting for ~ 63% of the protein sequence, *SI Appendix*, Fig. S1*A*). Recently, we and others reported that despite carrying the same amount of charge (+1e), arginine side chains are distinct compared to lysine as they are uniquely capable of mediating a hierarchy of ionic, cation-π, and π-π interactions with RNA (19, 26). To probe whether multi-modal Arg-RNA interaction is required for hollow condensate formation, we first tested whether a lysine variant of protamine (PRM-K; all 21 arginine residues are mutated to lysine, *SI Appendix*, Fig. S1*B*) can also form similar vesicular structures. Confocal microscopy imaging revealed a robust formation of stable hollow condensates for PRM-K under similar mixture compositions (Fig. 2*E*). Therefore, the ability to form vesicle-like assemblies is not dependent on the identity of the positively charged residues in nucleoproteins.

Both PRM and PRM-K have a high charge density [net charge per residue (NPCR) = 0.63]. To test whether high charge density is a prerequisite for vesicular condensate formation, we next used another naturally occurring cationic polypeptide, the RGG3 domain of FUS ($FUS^{472\text{-}504}$), which is similar in length to PRM but only contain 7 positive charges (NPCR = 0.2, see *SI Appendix*, Fig. S1*C*). Similar to the PRM system, FUS^{RGG3} also formed hollow condensates at excess RNA conditions (Fig. 2*F*). In all these systems, both proteins and RNAs showed co-localization in the rim, similar to PRM-RNA vesicle membranes. Together, these results highlight the generality of vesicular structure formation in mixtures of oppositely charged polypeptides and RNAs. Based on our previous studies on the condensate physical properties for arginine-to-lysine variants of R/G-rich proteins (19), we speculate that polypeptide primary sequence will tune the compositions at which vesicular assemblies are stable as well as the physicochemical properties of the vesicle rim. However, as discussed in the following section, the ability of these systems to spontaneously form hollow condensates appears to be generic under charge disproportionate conditions and is linked to the polyelectrolyte nature of the associative biopolymers.

Intra-complex charge disproportionation drives the formation of protein-RNA vesicles

Our phase diagram analysis of PRM-RNA system clearly indicate that vesicular structures are formed upon complexation between positively charged disordered polypeptide and negatively charged RNA under distinct charge disproportionate conditions (Fig. 2*A*). Many theories of polyelectrolyte complexation have predicted the existence of micellar and lamellar phases (27-31), but none of these theories predict hollow condensate formation as a function of the mixture composition. To conceptualize this phenomenon, we turn to the reentrant phase transition model for a mixture of oppositely charged polyelectrolytes by Shklovskii and Zhang (32). This model postulates that at conditions far from the charge neutral stoichiometry, mixtures of a long polyanion and a short polycation will form a charge disproportionate complex with a *tadpole-like* geometry consisting of a neutral head and a charged tail (Fig. 3*A*; *top* panels). The tadpole head can be considered as a nano-condensate. We propose that, as the concentration of tadpoles increases, heads of neighboring tadpoles may undergo surface tension-driven coalescence to form small spherical condensates (referred to as *micelles* henceforth), where the surfaces are decorated with the bare segments of RNA chains (Fig. 3*A*; *middle* panels; *SI Appendix*, Fig. S8). Although these micellar condensates are fluid-like (*SI Appendix*, Fig. S9), they are stabilized against coalescence-driven growth due to their highly negatively charged surfaces that are decorated by

RNAs (*SI Appendix*, Fig. S6). Upon further increase in the total concentration of micelles, the repulsion between RNA chains on the condensate surface becomes too large, triggering a micelle-to-vesicle transition. These vesicular condensates provide an additional internal surface allowing redistribution of bare RNA chains, thereby reducing the net repulsive energy (Fig. 3*A bottom* panels).

Although the Shklovskii-Zhang model can qualitatively explain the vesicle formation in RNA-protein mixtures as discussed above, the model only proposes tadpoles but not vesicles. To test whether tadpole-like complexes can self-assemble into vesicular structures, we performed molecular dynamics (MD) simulations using two oppositely charged chains that represent PRM and RNA. Amino acid residues and nucleic acid bases in these chains were represented as single beads (Fig. 3*B*). The interatomic potential employed in our simulations contain bonded, electrostatic, and short-range pairwise interaction terms as shown in Figure 3*B*. The simulation setup and the coarse-grained model employed is discussed in *SI Appendix, Materials and Methods*. The MD simulations were performed with $C_{RNA} = 5 \times C_{PRM}$ at three different RNA concentrations (0.01 mg/ml, 7.4 mg/ml and 15.80 mg/ml) that mimic the three experimental conditions. The system size ranges from 10^3-10^6 particles across the studied concentrations. The representative equilibrium structures sampled from MD simulations at these three concentrations are shown in Figure 3*C*. In our MD simulations, we find that charge disproportionate mixtures indeed form tadpole-like structures at low chain volume fraction, negatively charged micellar condensates at intermediate volume fraction, and hollow vesicle-like structures at relatively high volume fraction (Fig. 3*C*). Therefore, we infer that a vesicle-like phase is intrinsically accessible to oppositely charged polyelectrolyte mixtures under substantially charge disproportionate compositions. The simulation-derived density profiles of the PRM and RNA chains in the hollow vesicle-like structure is shown Figure 3*D* and is comparable to the experimental density profile shown in Figure 1*D*. To compare the relative diffusivities in various phases, we tag a single particle on the outside, the lumen, and the rim of the vesicle and follow its motion over a 10 ns segment of MD trajectory. The trajectories of these tagged particles are shown in Fig. 3*E*. We observe that the particles in the lumen and outside the vesicle have comparable diffusivities as they diffuse over a significant volume, indicating a low-density phase. Contrastingly, the particle within the rim has a much slower diffusivity and is confined close to its initial position, indicating a condensed phase. These results are consistent with our experimental FCS autocorrelation curves shown in Figure 1*E*.

Analogous to the excess RNA simulations, we also performed MD simulations with $C_{PRM} = 5 \times C_{RNA}$ at three different PRM concentrations (0.01 mg/ml, 7.0 mg/ml and 14.60 mg/ml). We find that akin to excess RNA conditions, the system equilibrates to tadpole-like structures at low concentration, positively charged condensates at intermediate concentration, and hollow vesicle-like structures at high concentration in excess PRM regimes (*SI Appendix*, Fig. S10*A*). We also observe that the vesicle has high density of PRM and RNA chains at the rims and has a low PRM concentration in its lumen (*SI Appendix*, Fig. S10*B*). This is similar to the density profile observed in vesicles formed at excess RNA conditions (Fig. 3*D*).

Both biological and synthetic polyelectrolyte systems can form hollow condensates at charge disproportionate mixture compositions

Our experimental observations and MD simulation results collectively suggest that vesicle formation might be an intrinsic feature of oppositely charged polyelectrolyte mixtures that undergo

complex coacervation, *e.g.*, liquid-liquid phase separation driven by heterotypic electrostatic interactions (33). To experimentally verify this idea, we tested the ability to form vesicles by several pairs of oppositely charged biological and synthetic polyelectrolytes. First, we kept the polycation (PRM) unchanged and changed the identity of the polyanion. We observed that PRM can form vesicle-like hollow condensates with inorganic polyphosphate (polyP), polyglutamic acid [poly(E)], and poly(acrylic acid) (PAA) at a similar charge disproportionate regime (Fig. 4*A-C, SI Appendix, Fig. S11*). Second, we changed the polycation, keeping the polyanionic RNA unchanged. Similar to the PRM-poly(U) system, we observe that the RNA can also form hollow condensates upon interaction with a synthetic cationic polyelectrolyte, poly(Allylamine) (PAH) under similar conditions (Fig. 4*D, SI Appendix, Fig. S11*). We also changed identities of both polycation and polyanion, and observed that PAH-polyP mixture form vesicles at charge disproportionate mixture compositions (Fig. 4*E, SI Appendix, Fig. S11*). Finally, we tested whether cellular RNA, a mixture that contains both structured and unstructured RNAs, can form vesicular assemblies. Indeed, we observed that total RNA from *Saccharomyces cerevisiae* can form stable micron-sized hollow condensates upon interaction with an R/G-rich polypeptide at excess RNA condition (Fig. 4*F, SI Appendix, Fig. S11*). These results reveal that vesicular assemblies represent a distinct yet generic condensed phase in biological as well as synthetic polyionic coacervates.

Protein-RNA hollow condensates exhibit molecular ordering, size-dependent permeability, and selective encapsulation

Oppositely charged disordered biopolymers attract each other through electric monopoles that are typically isotropic, *i.e.*, that they lack spatial directionality (34). However, in the case of amphiphiles, hydrophobic tail groups are packed together in the bilayer interior, which may give rise to spatial ordering in 2-dimensions. In the mesoscale, many amphiphilic assemblies, such as vesicles, are therefore characterized by a liquid crystalline ordering (35, 36). Our MD simulation results, however, suggest that the rims of the polyelectrolyte vesicles contain alternating bands of positively charged and negatively charged residues interspersed with the neutral residues of the PRM chains (*SI Appendix*, Fig. S10*C* and *D*). This organization of protein and RNA chains may result in local molecular ordering in protein-RNA vesicle membranes. To test the existence of ordered molecular organization experimentally, we imaged the PRM-RNA vesicles utilizing polarization light microscopy. Interestingly, we observed that PRM-RNA hollow condensates exhibited signatures of liquid-crystalline ordering on the rim (37) (Fig. 5*A*), whereas PRM-poly(U) droplets showed no signature ordering under similar conditions (*SI Appendix*, Fig. S12*A*). To check whether the ordering is specific to PRM-RNA vesicles, we recorded polarization micrographs of PRM-K–RNA, FUS^{RGG3}-RNA, and PRM-polyP vesicles (*SI Appendix*, Fig. S12 *B-D*). All these vesicles demonstrated an optical birefringent pattern, which is characteristic of molecular ordering in the rim (37). Therefore, our cross-polarization light microscopy images of polyionic vesicles suggest that molecular ordering in the rim is generic to polyelectrolyte vesicles, as is the case for many amphipathic lipid-membranes.

Our data indicate that physicochemical properties of the nucleoprotein vesicle rim are similar to nucleoprotein droplets (Fig. 1*F-G*). Recently, it was reported that ribonucleoprotein droplets can act as a size-dependent filter allowing permeability of molecules that are smaller than the condensate mesh-size (38). To test whether protein-RNA vesicle membranes have similar size-dependent permeability, we added fluorescently labeled dextran probes of various sizes to pre-formed hollow condensates. We observed that Dextran-4.4k (MW 4400 Da) partitioned favorably

within the rim, whereas a larger dextran, Dextran-10k, weakly partitioned to the rim. Further increase in the dextran size resulted in probe exclusion from both the rim and the lumen (Fig. 5*B*, *SI Appendix* Fig. S13). A summary of these results is presented in Figure 5*C,* where we plotted the partition coefficients in the rim/lumen for dextrans of different molecular weights ranging from 4.4k to 155k. These experiments suggest that, similar to ribonucleoprotein droplets, PRM-RNA hollow condensate rims act as a size-dependent filter. Based on the hydrodynamic radius of Dextran-10k in an aqueous buffer (38), we estimate the mesh-size of PRM-RNA vesicles to be ~ 2.3 nm.

A major application of amphiphilic vesicles is in cargo trafficking and delivery, which require entrapment of the cargo molecules within the internal vesicular lumen. We, therefore, tested the ability of protein-RNA vesicles to encapsulate a wide variety of client biomolecules (*e.g.*, proteins and nucleic acids). Using two-color confocal imaging, we determined partition coefficient for each client (defined as $I_{lumen}/I_{outside}$). We observed that both ssDNA and dsDNA are enriched within the lumens of PRM-RNA vesicles (Fig. 5*D*). For proteins, we observed that biomolecule loading into PRM-RNA vesicle is protein-specific. For example, bovine serum albumin (BSA) and the prion domain of FUS (PrD) were enriched in the PRM-RNA vesicle lumen whereas the green fluorescent protein (GFP) remains excluded. These results suggest that the PRM-RNA vesicles selectively enrich biomolecules and indicate a potential utility of these vesicles as stimuli responsive dynamic cargo carriers.

Conclusion

Heterotypic interactions between cationic R/K-rich LCDs and negatively charged RNAs have been shown to be crucial for the biomolecular condensation of many nucleoproteins (8, 39-41). Previously, we showed that RNA has a stoichiometry-dependent effect on the LLPS of these cationic LCDs [*i.e.,* at low RNA levels, LLPS of R/K-rich LCDs is facilitated and at high RNA levels, their LLPS is inhibited (18, 19)]. Here, we show that charge disproportionate nucleoprotein-RNA complexes can form distinct stable supramolecular topologies, such as tadpoles, micelles and vesicles. Our observed nucleoprotein vesicles bear significant structural and functional similarities with lipid vesicles. For example, similar to lipid membranes, nucleoprotein-RNA vesicle membranes exhibit molecular ordering and is able to selectively encapsulate biomolecules. However, unlike lipid vesicles, nucleoprotein vesicles remain highly dynamic and can readily undergo reversible *vesicle-to-droplet* phase transition in a stimuli responsive fashion. Thus, nucleoprotein vesicles may represent a dynamic mode of creating multilayered membrane-less assemblies that are ubiquitous in the subcellular space.

Physicochemically, the rims of nucleoprotein vesicles are similar to nucleoprotein droplets. As in the droplets, biomolecules in the rim are mobile and the rims of two vesicles in contact can undergo fusion. Our results suggest that the vesicular topology is thermodynamically stabilized by providing a greater surface area for the redistribution of unsatisfied charged tails of disproportionate protein-RNA complexes. We observe that the formation of vesicles is not specific to nucleoprotein-RNA complexes, rather is more generic to electrostatically driven complex coacervate systems. The geometric anisotropy of individual building blocks has been suggested to be a key driver for the "bottom-up" self-assembly of vesicular structures (42). For example, lipids and lipid-inspired di-block polymers that are known to form vesicles feature anisotropic architecture with two distinct domains, which vastly differ either in their solvent interactions or in their intermolecular inter-domain interactions (42, 43). Polyionic low-complexity polymers utilized in our current study, however, are intrinsically isotropic in isolation. Based on the

Shklovskii-Zhang model and our MD simulation, we propose that charge disproportionate complexes of isotropic polyelectrolytes can form anisotropic building blocks (such as tadpoles) that lead to vesicular assemblies. This opens up a new avenue to design and fabricate complex coacervate-based supramolecular assemblies with tunable topologies.

We envision several key implications of our observations. First, nucleoprotein condensates can attain multilayered topologies via the vesicle formation pathway. This pathway is orthogonal to the recently proposed mechanism of multiphasic condensate formation via coexisting liquid droplets in a multi-component mixture (5). Second, stimuli responsive sequestration through the dynamic formation/dissolution of vesicles of oppositely charged low-complexity polymers may have been utilized by prebiotic and protobiotic systems. Third, by coupling with stronger physical and/or chemical cross-linking strategies, polyelectrolyte vesicles can be utilized as stimuli responsive lipid-free cargo delivery systems for biotechnological applications (*e.g.,* drug/gene delivery, insecticide/pesticide release). These cargo delivery systems can be formulated carrier-free by directly utilizing proteins or nucleic acids of interest and therefore, achieve a high degree of target loading. Finally, these dynamic assemblies can be utilized to fabricate novel stimuli responsive microscale systems.

Figures and Legends

FIGURE-1

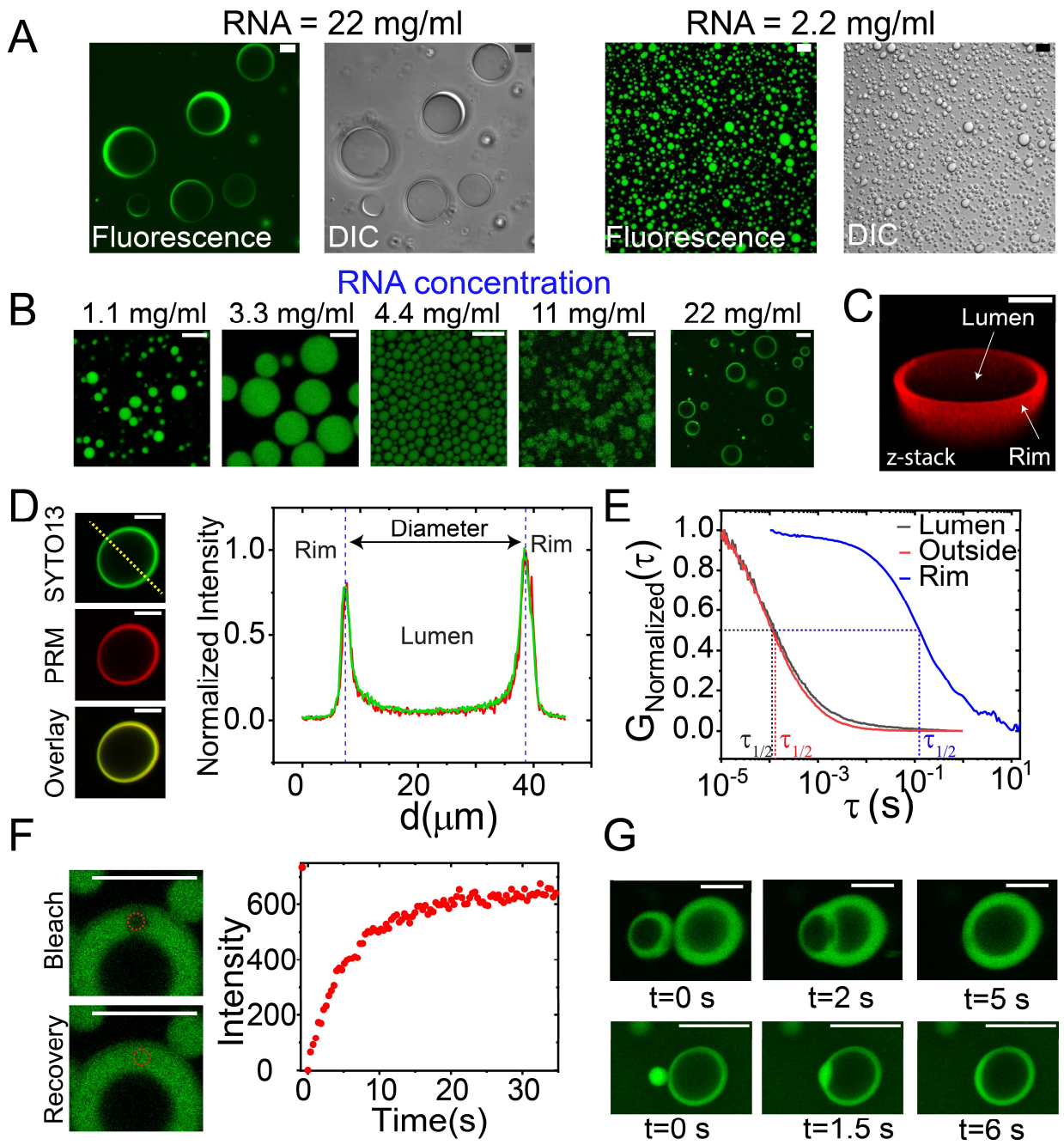

Figure 1: Protamine-RNA mixtures can form vesicular assemblies. ***(A)*** Fluorescence and DIC micrographs of PRM-RNA vesicles formed at 4.4 mg/ml PRM and 22 mg/ml poly(U) RNA (*i.e.*, [PRM] = 5 ×[RNA]; *left* panels). Contrastingly, at a lower PRM-to-RNA ratio, PRM-RNA mixtures form isotropic liquid droplets. Shown in *right* panels are micrographs of samples prepared upon mixing 4.4 mg/ml PRM and 2.2 mg/ml poly(U) RNA (*i.e.*, [PRM] = 0.5 × [RNA]).

(B) Fluorescence micrographs showing that mixture composition governs PRM-RNA droplets and vesicles formation. PRM concentration was fixed at 4.4 mg/ml. ***(C)*** 3D reconstruction of a PRM-RNA vesicle. ***(D)*** RNA (probed using SYTO13) and PRM (probed using Alexa594-labeled PRM) localize within the vesicle rim while the lumen has a hollow appearance. Fluorescence intensity of the lumen is similar to the external dilute phase. ***(E)*** Fluorescence correlation spectroscopy (FCS) autocorrelation curves for freely diffusing TMR-labeled Dextran-4.4k in three regions: inside the lumen, within the rim, and outside the hollow condensate. These autocorrelation curves suggest macromolecular diffusion is significantly slowed down (autocorrelation decays at ~100 ms) within the rim as compared to the lumen and the external dilute phase (autocorrelation decays at ~100 μs). ***(F)*** FRAP images and the corresponding intensity time-trace show near complete fluorescence recovery of the hollow condensate rim. The red circle indicates the bleaching region (also see Supplementary Movie 1). ***(G)*** Optical tweezer-controlled fusion of two PRM-RNA hollow condensates (*top* panels) and a PRM-RNA droplet with a hollow condensate (*bottom* panels) (see also corresponding Supplementary Movies 2 and 3, respectively). Experiments were performed in 25 mM Tris-HCl buffer (pH 7.5). Fluorescent probe concentrations were ≤ 1% of the unlabeled protein and RNA. Scale bars represent 10 μm.

FIGURE-2

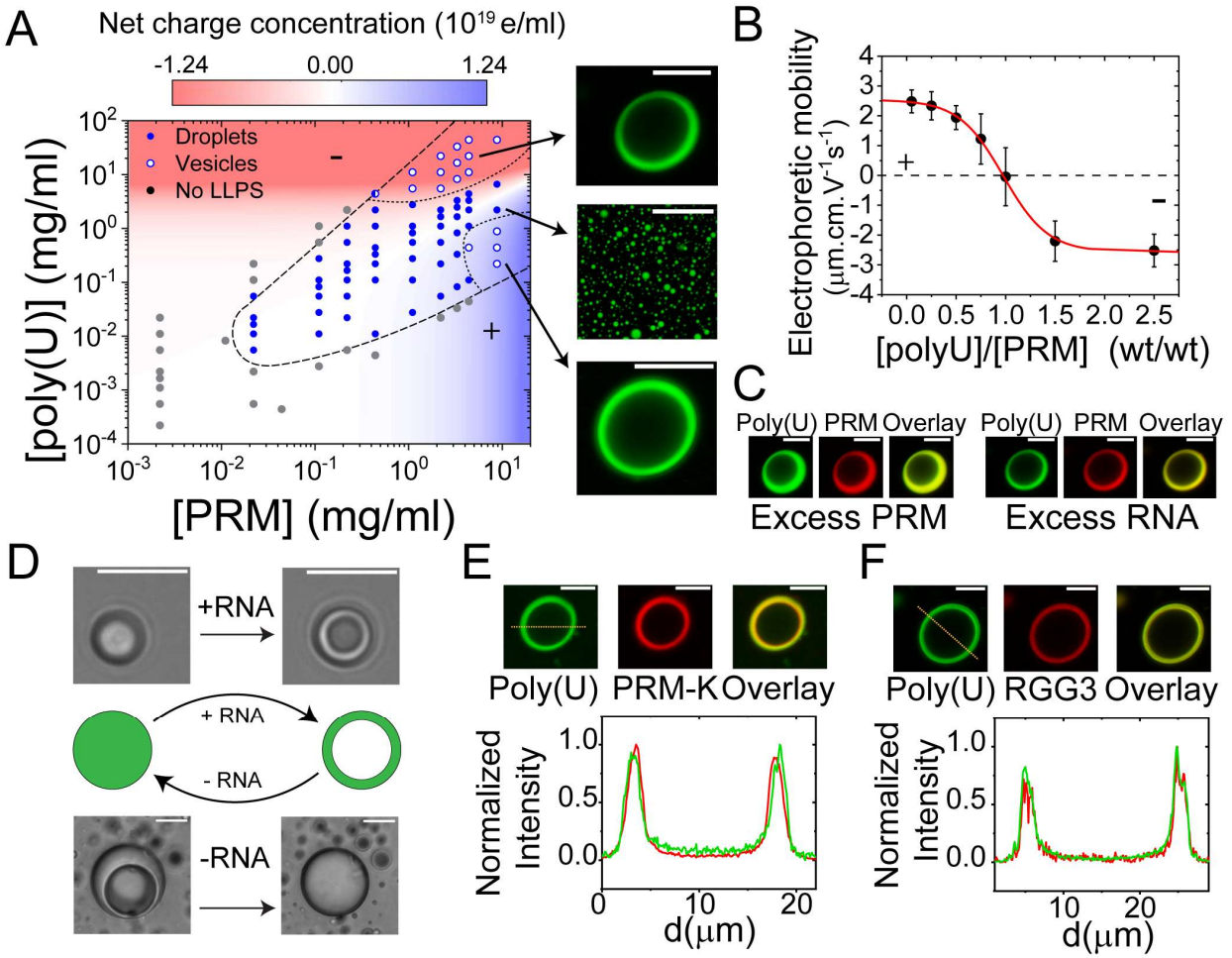

Figure 2: Vesicle-like polypeptide-RNA condensate is a thermodynamically stable phase. ***(A)*** Phase diagram of PRM-poly(U) mixture shows three distinct phases: a homogeneous state (filled gray circles), PRM-poly(U) isotropic liquid droplets (filled blue circles), and PRM-poly(U) vesicles (open blue circles). The dashed line represents the boundary between homogeneous and phase separated regimes. The background colored shade represents the estimated concentration of electric charge (calculated from mixture composition). Hollow condensates were present at two narrow regimes within this phase diagram, as indicated by dotted lines. ***(B)*** Electrophoretic mobility measured by dynamic light scattering of PRM-poly(U) condensates as a function of poly(U)-to-PRM ratio. This data clearly shows charge inversion: condensates have a net positive charge at low RNA-to-PRM ratio and a net negative charge at high RNA-to-PRM ratio. PRM concentration was 1.1 mg/ml for this experiment. ***(C)*** Fluorescence micrographs of hollow condensates at RNA excess (upper edge of the LLPS region in ***A***) and PRM excess (lower edge of the LLPS region in ***A***) conditions. The excess PRM sample was prepared at 8.8 mg/ml PRM and 0.44 mg/ml poly(U). The excess RNA sample was made at 4.4 mg/ml PRM and 22 mg/ml poly(U). ***(D)*** A scheme showing droplet-to-vesicle and vesicle-to-droplet transformations upon RNA influx and removal, respectively (*middle* panels). DIC images of a PRM-RNA droplet [0.88 mg/ml PRM, 0.44 mg/ml poly(U)] transitioning to a vesicle upon RNA influx (*top* panels; also see *SI Appendix*

Fig. S7 for experimental details; Supplementary Movie 4). DIC images of a PRM-RNA vesicle transitioning to a homogeneous droplet as a result of RNA removal (RNase-A treatment; *bottom* panels; see also Supplementary Movie 5). Fluorescence micrographs (*top* panels) and corresponding intensity profiles (*bottom* panels) of **(*E*)** hollow condensates formed by PRM-K (4.4 mg/ml) and poly(U) RNA (22 mg/ml), and ***(F)*** FUS^{RGG3} (4.0 mg/ml) and poly(U) RNA (20 mg/ml). Scale bars are 10 µm.

FIGURE-3

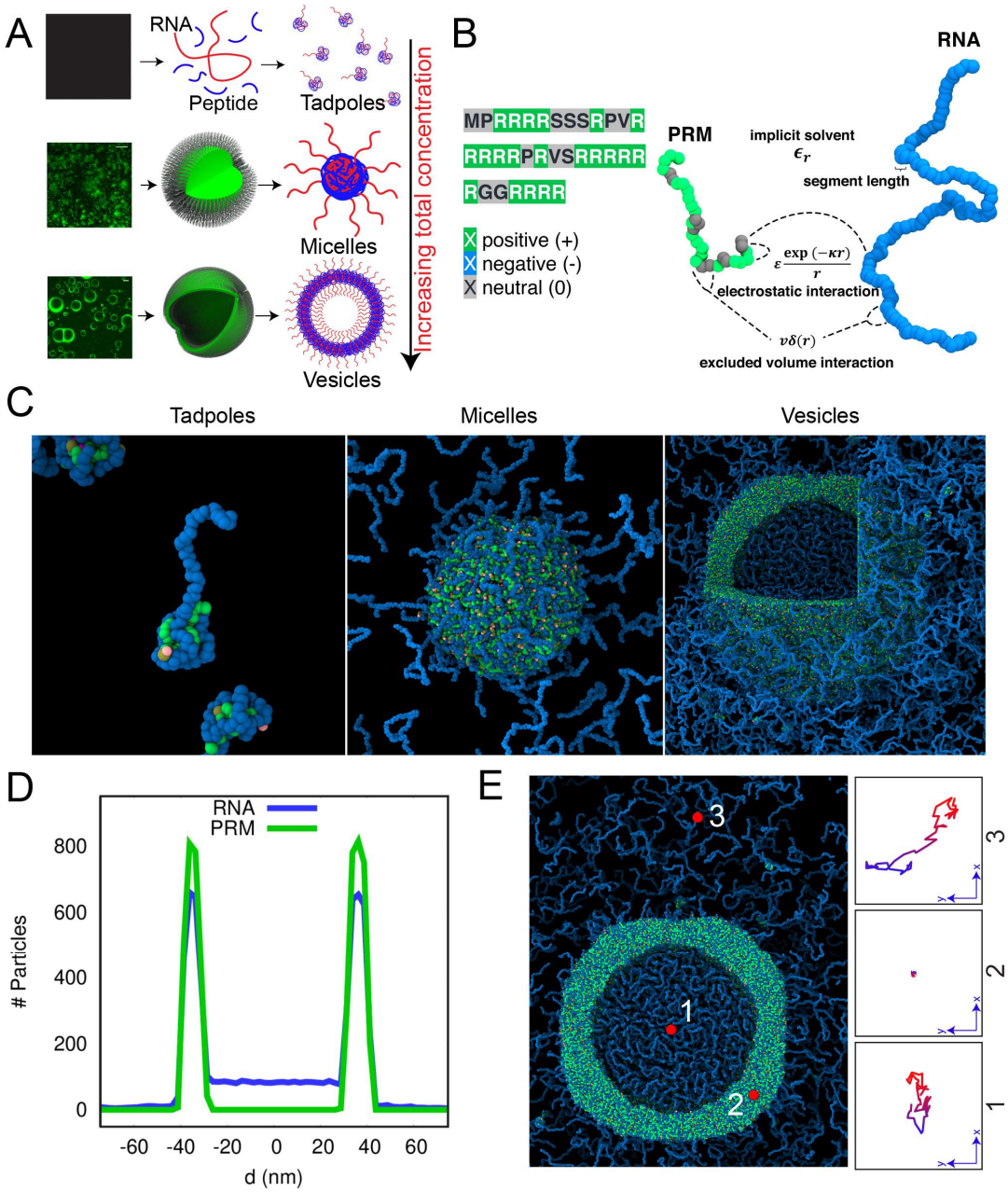

Figure 3: Charge disproportionation drives the formation of vesicular assemblies. ***(A)*** A scheme for the formation of RNA-protein hollow condensates based on the Shklovskii-Zhang model. Left column panels show representative experimental observations (fluorescence micrographs). The proposed mechanism is shown in right two columns. At low concentrations, nucleoprotein-RNA mixtures form tadpole-like complexes. Increasing the total concentration leads to the formation of small spherical micellar assemblies. At relatively high total concentration, nucleoprotein-RNA vesicular structures are formed. ***(B)*** Schematic representation of the protein and RNA chains and the interaction potential employed in our molecular dynamics (MD) simulations. ***(C)*** Equilibrium MD configurations showing tadpole, micelle, and vesicle formed under charge disproportionate conditions, $C_{RNA} = 5 \times C_{PRM}$. (***D***) Density profiles of PRM and RNA chains for the vesicle obtained

from the MD trajectory. ***(E)*** Diffusion trajectories of a tagged particle (red sphere) located within the lumen, within the rim, and outside of the vesicle.

FIGURE-4

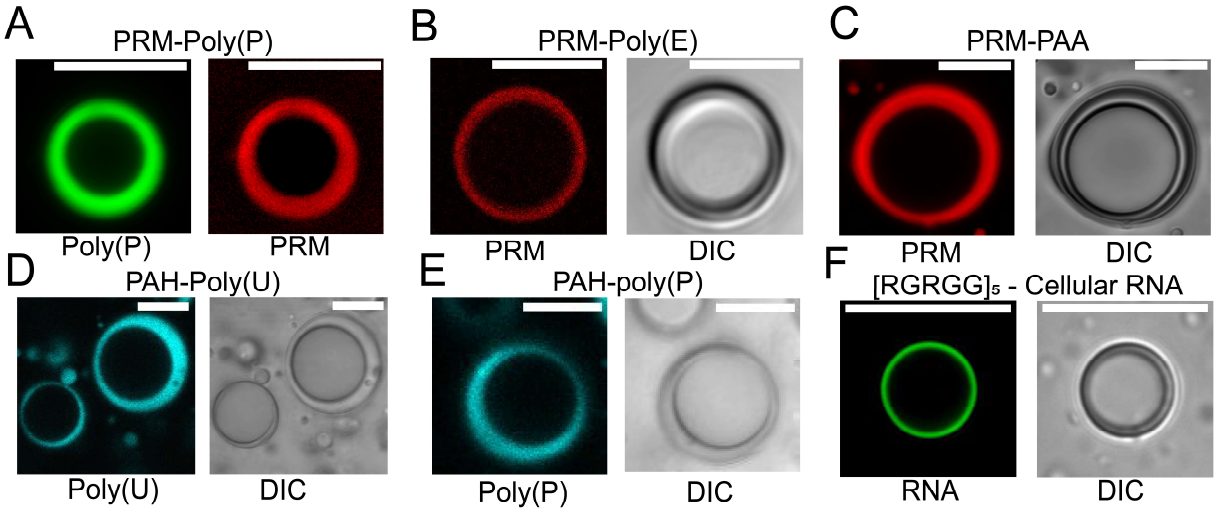

Figure 4. Both biological and synthetic polyionic chains can form vesicles. Fluorescence and DIC micrographs of hollow condensates formed by PRM (4.4 mg/ml) and polyP (22.0 mg/ml, ***A***); PRM (17.6 mg/ml) and poly(E) (18 mg/ml, ***B***); PRM (8.8 mg/ml) and poly(acrylic acid) (PAA; 22 mg/ml, ***C***); PAH (40 mg/ml) and poly(U) (4.0 mg/ml, ***D***); PAH (70 mg/ml) and polyP (4 mg/ml, ***E***); and $[RGRGG]_5$ (0.024 mg/ml) and cellular RNA (8.9 mg/ml, ***F***). See also *SI Appendix* Figure S11. Scale bars represent 10 μm.

FIGURE-5

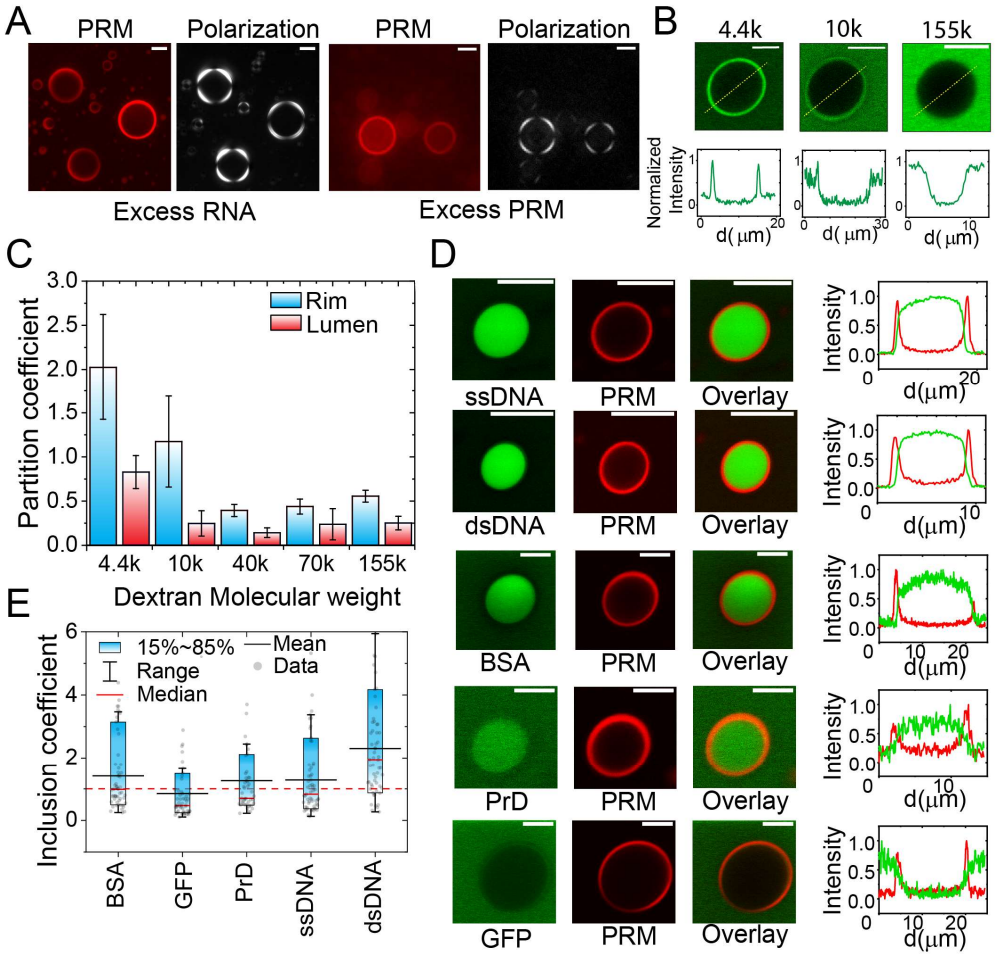

Figure 5: PRM-RNA hollow condensate rims exhibit membrane-like properties. ***(A)*** Optical images of PRM-RNA hollow condensates with cross-polarizing light show birefringence, indicating molecular ordering in the vesicle rims. Corresponding fluorescence micrographs are also shown. ***(B)*** Fluorescence images and corresponding intensity profiles of TMR-labeled dextran probes of different molecular weights reveal size-dependent partitioning in PRM-RNA hollow condensates. The low molecular weight dextran, Dex-4.4k, partitions to the rim whereas the high molecular weight dextran, Dex-155k, remains excluded from the rim. See also *SI Appendix* Figure S13. ***(C)*** A bar plot of size-dependent partitioning data of dextrans into the rim and lumen of PRM-RNA hollow condensates. ***(D)*** Partitioning of nucleic acids and proteins into PRM-RNA vesicles. The intensity profiles are measured along a horizontal line passing through the center of individual hollow condensates. *BSA*: Bovine Serum Albumin; *GFP*: Green Fluorescent Protein; *PrD*: Prion-like domain of FUS. ***(E)*** Inclusion coefficients (defined as the ratio of *mean intensity in the lumen* to *mean intensity in the external dilute phase*) are shown. The statistics were estimated using a minimum of 50 different hollow condensates per sample. Individual points are shown as gray filled circles. Scale bars are 10 μm.

Acknowledgements

The authors gratefully acknowledge UB north campus confocal imaging facility (supported by National Science Foundation MRI Grant: DBI 0923133) and its director, Mr. Alan Siegel for helpful assistance. The authors also acknowledge helpful discussions with Ms. Taranpreet Kaur and Dr. Wei Wang at various stages of manuscript preparation.

Funding

We gratefully acknowledge support for this work from University at Buffalo, SUNY, College of Arts and Sciences to P.R.B. and funding from the National Institute on Aging (NIA) of the National Institutes of Health (R21 AG064258) to P.R.B.

Author contributions

P.R.B. and M.M.M. conceived the idea. I.A. and P.R.B. designed the experiments. I.A. preformed the experiments and analyzed the data with help from P.R.B. M.R. and D.P. designed and performed the MD simulation. P.R.B., M.M.M., and I.A. wrote the manuscript with input from M.R. and D.P.

References

1. van Meer G, Voelker DR, & Feigenson GW (2008) Membrane lipids: where they are and how they behave. *Nat. Rev. Mol. Cell Biol.* 9(2):112-124.
2. Banani SF, Lee HO, Hyman AA, & Rosen MK (2017) Biomolecular condensates: organizers of cellular biochemistry. *Nat Rev Mol Cell Biol* 18(5):285-298.
3. Boeynaems S*, et al.* (2018) Protein Phase Separation: A New Phase in Cell Biology. *Trends Cell Biol.* 28(6):420-435.
4. Gomes E & Shorter J (2019) The molecular language of membraneless organelles. *J Biol Chem* 294(18):7115-7127.
5. Shin Y & Brangwynne CP (2017) Liquid phase condensation in cell physiology and disease. *Science* 357(6357).
6. Li X-H, Chavali PL, Pancsa R, Chavali S, & Babu MM (2018) Function and Regulation of Phase-Separated Biological Condensates. *Biochemistry* 57(17):2452-2461.
7. Brangwynne CP, Tompa P, & Pappu RV (2015) Polymer physics of intracellular phase transitions. *Nat Phys* 11(11):899-904.
8. Feric M*, et al.* (2016) Coexisting Liquid Phases Underlie Nucleolar Subcompartments. *Cell* 165(7):1686-1697.
9. Fei J*, et al.* (2017) Quantitative analysis of multilayer organization of proteins and RNA in nuclear speckles at super resolution. *J. Cell Sci.* 130(24):4180-4192.
10. West JA*, et al.* (2016) Structural, super-resolution microscopy analysis of paraspeckle nuclear body organization. *The Journal of Cell Biology* 214(7):817-830.
11. Jain S*, et al.* (2016) ATPase-Modulated Stress Granules Contain a Diverse Proteome and Substructure. *Cell* 164(3):487-498.
12. Cirillo L, Cieren A, & Gotta M (2019) Molecularly distinct cores coexist inside stress granules. *bioRxiv*:663955.
13. Putnam A, Cassani M, Smith J, & Seydoux G (2019) A gel phase promotes condensation of liquid P granules in Caenorhabditis elegans embryos. *Nat. Struct. Mol. Biol.* 26(3):220-226.
14. Arkov AL, Wang J-YS, Ramos A, & Lehmann R (2006) The role of Tudor domains in germline development and polar granule architecture. *Development* 133(20):4053-4062.
15. Mahowald AP (1962) Fine Structure of Pole Cells and Polar Granules in Drosophila Melanogaster. *J. Exp. Zool.* 151(3):201-&.
16. Kistler KE*, et al.* (2018) Phase transitioned nuclear Oskar promotes cell division of Drosophila primordial germ cells. *Elife* 7.
17. Schmidt HB & Rohatgi R (2016) In Vivo Formation of Vacuolated Multi-phase Compartments Lacking Membranes. *Cell Rep* 16(5):1228-1236.
18. Banerjee PR, Milin AN, Moosa MM, Onuchic PL, & Deniz AA (2017) Reentrant Phase Transition Drives Dynamic Substructure Formation in Ribonucleoprotein Droplets. *Angew Chem Int Ed Engl* 56(38):11354-11359.
19. Alshareedah I*, et al.* (2019) Interplay between Short-Range Attraction and Long-Range Repulsion Controls Reentrant Liquid Condensation of Ribonucleoprotein-RNA Complexes. *J Am Chem Soc* 141(37):14593-14602.
20. Mao AH, Crick SL, Vitalis A, Chicoine CL, & Pappu RV (2010) Net charge per residue modulates conformational ensembles of intrinsically disordered proteins. *Proc Natl Acad Sci U S A* 107(18):8183-8188.
21. Poot M, Gibson LL, & Singer VL (1997) Detection of apoptosis in live cells by MitoTracker red CMXRos and SYTO dye flow cytometry. *Cytometry* 27(4):358-364.
22. Almeida PFF & Vaz WLC (1995) Chapter 6 - Lateral Diffusion in Membranes. *Handbook of Biological Physics*, eds Lipowsky R & Sackmann E (North-Holland), Vol 1, pp 305-357.

23. Kulin S, Kishore R, Helmerson K, & Locascio L (2003) Optical Manipulation and Fusion of Liposomes as Microreactors. *Langmuir* 19(20):8206-8210.
24. Phillips R, Theriot J, Kondev J, & Garcia H (2012) *Physical biology of the cell* (Garland Science).
25. Choi JM, Dar F, & Pappu RV (2019) LASSI: A lattice model for simulating phase transitions of multivalent proteins. *PLoS Comput Biol* 15(10):e1007028.
26. Boeynaems S*, et al.* (2019) Spontaneous driving forces give rise to protein-RNA condensates with coexisting phases and complex material properties. *Proc Natl Acad Sci U S A* 116(16):7889-7898.
27. Borisov O & Zhulina E (2003) Morphology of micelles formed by diblock copolymer with a polyelectrolyte block. *Macromolecules* 36(26):10029-10036.
28. Oskolkov NN & Potemkin II (2007) Complexation in asymmetric solutions of oppositely charged polyelectrolytes: Phase diagram. *Macromolecules* 40(23):8423-8429.
29. Shusharina NP & Rubinstein M (2007) Scaling theory of polyelectrolyte and polyampholyte micelles. *Nanostructured Soft Matter*, (Springer), pp 301-326.
30. Castelnovo M & Joanny J (2002) Phase diagram of diblock polyampholyte solutions. *Macromolecules* 35(11):4531-4538.
31. Castelnovo M (2003) Thermodynamics of micellization of oppositely charged polymers. *EPL (Europhysics Letters)* 62(6):841.
32. Zhang R & Shklovskii B (2005) Phase diagram of solution of oppositely charged polyelectrolytes. *Physica A: Statistical Mechanics and its Applications* 352(1):216-238.
33. Aumiller WM, Jr. & Keating CD (2016) Phosphorylation-mediated RNA/peptide complex coacervation as a model for intracellular liquid organelles. *Nat Chem* 8(2):129-137.
34. Israelachvili JN (2015) *Intermolecular and surface forces* (Academic press).
35. Jia L & Li M-H (2014) Liquid crystalline polymer vesicles: thermotropic phases in lyotropic structures. *Liquid Crystals* 41(3):368-384.
36. Kulkarni CV (2012) Lipid crystallization: from self-assembly to hierarchical and biological ordering. *Nanoscale* 4(19):5779-5791.
37. Mishima K, Satoh K, & Ogihara T (1987) Optical birefringence of phosphatidylcholine liposomes in gel phases. *Biochimica et Biophysica Acta (BBA) - Biomembranes* 898(2):231-238.
38. Wei MT*, et al.* (2017) Phase behaviour of disordered proteins underlying low density and high permeability of liquid organelles. *Nat Chem* 9(11):1118-1125.
39. Lin Y, Protter DS, Rosen MK, & Parker R (2015) Formation and Maturation of Phase-Separated Liquid Droplets by RNA-Binding Proteins. *Mol Cell* 60(2):208-219.
40. Molliex A*, et al.* (2015) Phase separation by low complexity domains promotes stress granule assembly and drives pathological fibrillization. *Cell* 163(1):123-133.
41. Mitrea DM*, et al.* (2016) Nucleophosmin integrates within the nucleolus via multi-modal interactions with proteins displaying R-rich linear motifs and rRNA. *Elife* 5.
42. Discher DE & Eisenberg A (2002) Polymer Vesicles. 297(5583):967-973.
43. Israelachvili J, Marčelja S, & Horn RG (1980) Physical principles of membrane organization. *Quarterly reviews of biophysics* 13(2):121-200.